International Journal of Engineering Science 49 (2011) 279–294

Contents lists available at ScienceDirect

International Journal of Engineering Science

journal homepage: www.elsevier.com/locate/ijengsci

Stress-function variational method for stress analysis of bonded joints under mechanical and thermal loads

Xiang-Fa Wu *, Robert A. Jenson

Department of Mechanical Engineering, North Dakota State University, Fargo, ND 58108-6050, USA

ARTICLE INFO

Article history:
Received 3 August 2010
Accepted 8 November 2010
Available online 8 January 2011

Keywords:
Interfacial stresses
Thermomechanical stress
Free-edge stress
Bonded joints
Stress function
Energy method
Elasticity

ABSTRACT

High interfacial stresses near the ends of adherends are responsible for debonding failure of bonded joints used extensively in structural engineering and microelectronics packaging. This paper proposes a stress-function variational method for determination of the interfacial stresses in a single-sided strap joint subjected to mechanical and thermal loads. During the process, two interfacial shear and normal (peeling) stress functions are introduced, and the planar stresses of adherends of the joints are expressed in terms of the stress functions according to the static equilibrium equations. Two coupled governing ordinary differential equations (ODEs) of the stress functions are obtained through minimizing the complementary strain energy of the joints and solved explicitly in terms of eigenfunctions. The stress field of the joints based on this method can satisfy all the traction boundary conditions (BCs), especially the shear-free condition near the adherend ends. Compared to results based on finite element method (FEM) and other analytic methods in the literature, the present variational method is capable of predicting highly accurate interfacial stresses. Dependencies of the interfacial stresses upon the adherend geometries, moduli and temperature are examined. Results gained in this study are applicable to scaling analysis of joint strength and examination of solutions given by other methods. The present formalism can be extended conveniently to mechanical and thermomechanical stress analysis of other bonded structures such as adhesively bonded joints, composite joints, and recently developed flexible electronics, among others.

1. Introduction

Bonded joints have found extensive applications in load transfer and connection of separated parts in aerospace, ground and marine vehicles and other broad mechanical and civil structures. Bonded joints also play an important role in microelectronics packaging and structural repairing. In the view of structural integrity, strength and durability of bonded joints directly influences the reliability and safety of the resulting structures. Due to the existence of multiple surfaces/interfaces and material dissimilarities across bonding interfaces, a complicated stress field and high stress concentration usually exist near free edges of bonded joints in service. The high interfacial shear and normal (peeling) stresses are responsible for the typical debonding failure of joints. Without a doubt, accurate estimate of the mechanical and thermal stresses of bonded joints is crucial to joint design and health evaluation as well as understanding of their failure mechanism and damage evolution.

In the past decades, several analytic joint models have been proposed to approach the stress field of bonded joints subjected to mechanical and thermal loads. To mention a few, Volkersen (1938) and Goland and Reissner (1944) are deemed as

* Corresponding author. Fax: +1 701 231 8913.
E-mail address: xiangfa.wu@ndsu.edu (X.-F. Wu).

0020-7225/$ - see front matter © 2010 Elsevier Ltd. All rights reserved.
doi:10.1016/j.ijengsci.2010.11.005

the pioneers who first conducted the stress analyses of adhesively bonded single-lap joints subjected to mechanical loads. A few limitations exist in their pioneering studies: the peak shear stress appears at adherend ends that violates the shear-free condition at the free-ends; stress variation across the adhesive layer was ignored, among others. Hart-Smith (1973a, 1973b) extended the above works by further taking into account the plasticity (idealized elastoplastic solid model) of the adhesive layer, adherend stiffness imbalance and thermal mismatch. In Hart-Smith's work, a failure criterion based on maximum shear-strain was adopted. It was concluded that plastic deformation of the adhesive layer enhanced the strength of adhesively bonded lap joints; in contrast dissimilarities of stiffness and coefficients of thermal expansion of the adherends decreased the strength of the bonded joints under consideration (Hart-Smith, 1973a, 1973b). Besides, by using a higher order theory, Chen and Cheng (1983) presented an analytic model based on two-dimensional (2D) elasticity and the theorem of minimum complementary strain energy. This model predicts that the peak shear stress in the adhesive layer is located at a distance of $\sim$20% the adherend thickness from the adherend ends. Such shear stress distribution is largely in an agreement with those predicted by means of finite element analysis (FEA) (Diaz, Hadj-Ahmed, Foret, & Ehrlacher, 2009; Lee & Kim, 2005; Mortensen & Thomsen, 2002). In addition, Tsai, Oplinger, and Morton (1998) furthered the classic studies by Volkersen (1938) and Goland and Reissner (1944) to adopt a linearly varying shear deformation across the adhesive layer. Her (1999) provided a simple tension-bar model to approach the interfacial stresses in adhesively bonded lap joints; Lee and Kim (2005) considered adhesively bonded single/double lap joints, in which the adhesive layers were modeled as distributed linearly elastic springs. Similarly, a generalized treatment dealing with the adherends as flexural beams can be traced to an earlier work by Delale, Erdogan, and Aydinoglu (1981). A detailed review of historical development and comparison of several important analytical models for stress analysis of adhesively bonded joints and composite joints can be found in the recent review papers dedicated by da Silva, das Neves, Adams, and Spelt (2009a, 2009b). Yet, by studying the available models of adhesively bonded joints, it is obvious that the adhesive layers in these models play a crucial role in the modeling process and they function to connect the adherends of mismatching displacements. However, mismatch of material properties between the adherends and adhesive layers has been ignored though some thermosetting adhesive systems actually bear the moduli very close to those of the synthetic adherends; generalized Hooke's law of the adhesive layers and the shear-free condition at the ends of adherends are not satisfied in most of these models.

On the other hand, with the development of microelectronics techniques since the 1980s, thermal stress induced structural failure and functionality defects in electronics packaging have become one of the technical concerns attracting exceptional research in the last three decades (Chen & Nelson, 1979; Ru, 2002; Suhir, 1986, 1989a, 1989b, 1991, 2001; Suhir & Vujosevic, 2010; Suo, 2003; Timoshenko, 1925; Tsai, Hsu, & Han, 2004). It is technically desired to accurately predict the interfacial thermal stresses in bonded thermostats (chips) (Chen & Nelson, 1979; Ru, 2002; Suhir, 1986, 1989a, 1989b, 1991, 2001; Suhir & Vujosevic, 2010; Timoshenko, 1925; Tsai et al., 2004) and the failure mechanism and damage evolution in combined thermal and electric fields (Suo, 2003). More recently, with the birth of flexible electronics rooted in smart deposition of rigid silicon micro-devices on compliant polymeric substrates, substantial effort has been devoted to exploration of their mechanical functionality and durability that highly depend upon the interfacial stresses between the free-standing stiff silicon units and the flexible substrate layers (Jiang et al., 2007, 2008; Khang, Jiang, Huang, & Rogers, 2006, 2009; Kim & Rogers, 2008; Lu, Yoon, & Suo, 2007; Song et al., 2008; Sun, Choi, Jiang, Huang, & Rogers, 2006). Accurate prediction of such interfacial stresses is expected extremely important to optimize the deposition process and improve the mechanical durability of the novel intelligent flexible electronics to be commercialized in the near future (e.g. flexible displayers, etc.).

Along the vein of this development, in this study we propose an efficient stress-function variational method to approach the mechanical and thermomechanical stresses of bonded joints subjected to mechanical load and temperature change. Two interfacial shear and normal stress functions are introduced in this formulation; planar stress components of the bonded joints are expressed in terms of these stress functions. To do so, the axial normal stress in each adherend of the joints is assumed linearly varying across the adherend layer following the flexural stress formula of classic *Euler–Bernoulli* beams; the other planar shear and transverse normal stresses in the adherends are determined to satisfy the static equilibrium equations and traction boundary conditions at the bottom and top surfaces and the ends of the adherends. Based on the theorem of minimum complementary strain energy, two coupled governing ordinary differential equations (ODEs) of the stress functions can be obtained and solved explicitly in terms of eigenfunctions. The stress field of the joints given by this method can satisfy all the traction boundary conditions (BCs), especially the shear-free condition at the adherend ends which was normally ignored in typical analytic methods reported in the literature. Validation of the present method will be performed by comparison of the interfacial stresses with those predicted by finite element method (FEM) and other analytic methods. Dependencies of the interfacial stresses upon the adherend geometries, moduli and temperature change will be examined. The present method is expected to provide improved accuracy of stress analysis of bonded joints subjected to mechanical and thermal loads, which will further facilitate the study of interfacial cracking in bonded joints and other layered structures (Hutchinson & Suo, 1992; Li, 2001; Li & Lee, 2009; Sih, 1973; Suo & Hutchinson, 1990; Tada, Paris, & Irwin, 1973; Wu & Dzenis, 2002; Wu, Lilla, & Zou, 2002, 2003, 2003, 2004; Yu & Hutchinson, 2003; Yu, He, & Hutchinson, 2001). The rest of the paper is planned as follows. Section 2 provides the theoretical framework of the stress-function variational method based on a single-sided strap joint as used as the model joint, including expressions of adherend stresses in terms of the interfacial stress functions and formulation of the governing ODEs. Section 3 demonstrates the reliability of the present method through determining the stress field in a single-sided strap joint subjected to mechanical load and temperature change, respectively. Comparisons of the results with those given by FEM and available in the literature are made. Consequently, applications of the present formalism and conclusions of this study are remarked.

2. Problem formulation and solution

Without loss of generality, we start with a single-sided strap joint consisting of two identical slender substrate layers and a slender cover layer as sketched in Fig. 1. The cover layer has the length $2L$, thickness h_1, and width b, and the substrate layers have the thickness h_2, width b, and length much larger than L. The coordinate systems are introduced as follows. The x-coordinate is selected from the symmetric mid-span of the joint and directs along the layer axis; y_1 and y_2 are the vertical coordinates with the corresponding origins located at the centroids of cross-sections of the cover and substrate layers, respectively. The substrate layers are subjected to a uniform tensile stress p_0 far away the cover layer; meanwhile the joint is subjected to a uniform temperature change ΔT from the reference temperature of thermal stress free state. Due to symmetry of the joint and external loading, stress analysis of the joint can be made only on the right half-portion [see Fig. 1(b)]. It is expected that the mismatch of material properties across the adherend interfaces yields high mechanical and thermomechanical interfacial shear and normal stresses (debonding stresses) at the adherend ends as illustrated in Fig. 1(c). Such high interfacial stresses are responsible for the failure of bonded joints, such as interface debonding commonly observed in engineered structural joints.

Rigidly speaking, the adherends of bonded joints are in a complicated three-dimensional (3D) stress state due to the mismatch of Poisson's ratios across the adherend interfaces. To simplify the process, hereafter the joint is considered in the *plane-stress* state, no residual stresses exist in the initial load-free state at the reference temperature, and the temperature change is uniform in the joint. In addition, the adherends are dealt with as isotropic, linearly thermoelastic solids. For the convenience of derivation below, parameters and variables with subscripts 1 and 2 are attached to the cover layer and the substrate layers, respectively. Furthermore, results obtained in the *plane-stress* state can be conveniently converted to those of the *plane-strain* state by replacing the Young's moduli $E_i (i = 1,2)$ by $E_i/(1-\upsilon_i^2)$, Poisson's ratio $\upsilon_i (i = 1,2)$ by $\upsilon_i/(1-\upsilon_i)$, and coefficients of thermal expansion $\alpha_i (i = 1,2)$ by $(1+\upsilon_i)\alpha_i$.

2.1. Static equilibrium equations

Due to loss of lateral symmetry, deformation of a single-sided strap joint subjected to axial tension and/or uniform temperature change is a combination of in-plane elongation and lateral deflection. The adherends of the joint are slender and therefore dealt with as classic *Euler–Bernoulli* beams. Free-body diagrams (FBDs) of representative segments of the cover and the substrate layers are shown in Fig. 2(a) and (b), respectively, in which stresses and relevant resultants, i.e., the axial force S_i, shear force Q_i, and bending moment $M_i (i = 1,2)$, are defined to follow standard sign conventions designated in elementary *Mechanics of Materials* (Beer, Johnston, Dewolf, & Mazurek, 2009). For the representative segmental element of the cover layer [see Fig. 2(a)], relevant static equilibrium equations are

$$\Sigma F_x = 0 : \frac{dS_1}{dx} = -b\tau, \tag{1}$$

$$\Sigma F_y = 0 : \frac{dQ_1}{dx} = -b\sigma, \tag{2}$$

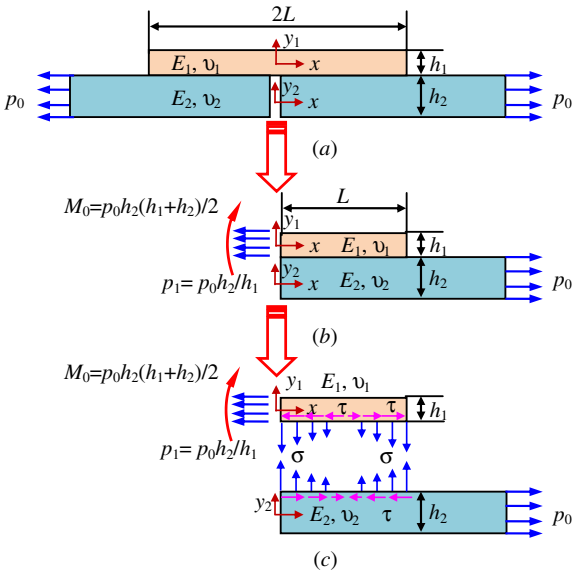

Fig. 1. Schematic of a single-sided strap joint: (a) the joint consists of a slender cover layer bonded to two identical slender substrate layers, (b) reduced right half-structure based on symmetry, and (c) schematic interfacial shear and normal stresses.

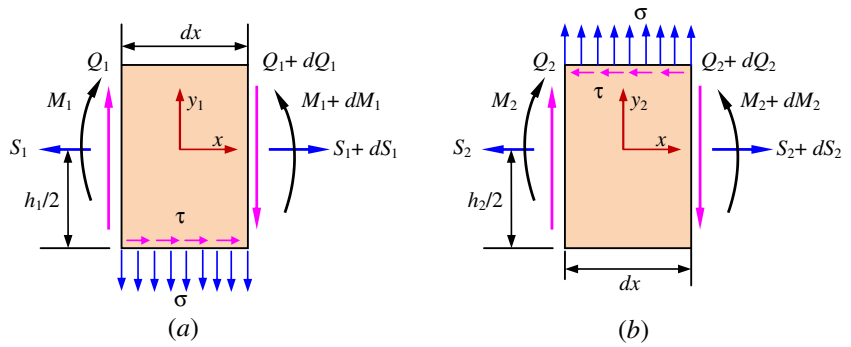

Fig. 2. Free-body diagrams of representative segmental elements of the adherends: (a) a representative segmental element of the cover layer and (b) a representative segmental element of the right-substrate layer.

$$\Sigma M = 0 : \frac{dM_1}{dx} = Q_1 - \frac{h_1}{2}(b\tau). \tag{3}$$

Meanwhile, the static equilibrium equations of the representative segmental element of the right-substrate layer [see Fig. 2(b)] are

$$\Sigma F_x = 0 : \frac{dS_2}{dx} = b\tau, \tag{4}$$

$$\Sigma F_y = 0 : \frac{dQ_2}{dx} = b\sigma, \tag{5}$$

$$\Sigma M = 0 : \frac{dM_2}{dx} = Q_2 - \frac{h_2}{2}(b\tau). \tag{6}$$

2.2. Stress resultants

Define the interfacial shear stress τ and normal (peeling) stress σ as two independent functions to be determined:

$$\tau = f(x) \text{ and } \sigma = g(x). \tag{7}$$

The shear-free condition of the adherend edges at $x = 0$ and L requires

$$f(0) = f(L) = 0. \tag{8}$$

In addition, physical conditions of the axial tractions, shear-forces and bending moments at the adherend ends of the joint specify

$$S_1(0) = p_0 b h_2, \tag{9a}$$
$$S_1(L) = 0, \tag{9b}$$
$$Q_1(0) = 0, \tag{9c}$$
$$Q_1(L) = 0, \tag{9d}$$
$$M_1(0) = M_0 = p_0 b h_2 (h_1 + h_2)/2, \tag{9e}$$
$$M_1(L) = 0. \tag{9f}$$
$$S_2(0) = 0, \tag{9g}$$
$$S_2(L) = p_0 b h_2, \tag{9h}$$
$$Q_2(0) = 0, \tag{9i}$$
$$Q_2(L) = 0, \tag{9j}$$
$$M_2(0) = 0, \tag{9k}$$
$$M_2(L) = 0. \tag{9l}$$

In the above, not all the BCs are linearly independent as will be discussed in Section 2.4.

In the case of thermomechanical stress analysis of the joint due to a pure temperature change $\Delta T(p_0 = 0)$, the right terms of (9a), (9e) and (9h) should be zeros in order to satisfy the traction-free BCs. In this case, thermomechanical analysis of a single-sided strap joint is equivalent to that of bi-material thermostats as initially studied by Timoshenko (1925) and Suhir (1986, 1989a, 1989b, 1991).

Furthermore, all the stress resultants of the segmental elements of the layers can be uniformly expressed in terms of f and g as follows. By integrating (1) with respect to x from $x = 0$, it yields

$$\int_0^x dS_1 = -\int_0^x bf(\xi)d\xi. \tag{10}$$

With the shear-free condition at $x = 0$, i.e., BC (8), and BC (9a), the axial normal force (10) in the cover layer can be written as

$$S_1(x) = p_0 bh_2 - b\int_0^x f(\xi)d\xi. \tag{11}$$

Integration of (2) with respect to x from $x = 0$ gives the shear-force of the cover layer:

$$\int_0^x dQ_1 = -\int_0^x bg(\xi)d\xi. \tag{12}$$

In addition, with the aid of the shear-free condition at $x = 0$ as given in (9c), the shear-force (12) in the cover layer becomes

$$Q_1(x) = -b\int_0^x g(\xi)d\xi. \tag{13}$$

Moreover, integration of (3) with respect to x from $x = 0$ gives

$$\int_0^x dM_1 = \int_0^x \left[Q_1(\xi) - \frac{h_1}{2}(b\tau)\right]d\xi. \tag{14}$$

By using the bending-moment BC at $x = 0$ as given in (9e), the bending moment (14) in the cover layer can be expressed

$$M_1(x) = M_0 - b\int_0^x \int_0^\xi g(\varsigma)d\varsigma\, d\xi - \frac{bh_1}{2}\int_0^x f(\xi)d\xi. \tag{15}$$

Based on the same procedure, integration of (4) with respect to x from $x = 0$ yields

$$\int_0^x dS_2 = \int_0^x bf(\xi)d\xi. \tag{16}$$

With the axial traction BC at $x = 0$ as given in (9g), the axial force (16) in the substrate layer can be expressed as

$$S_2(x) = b\int_0^x f(\xi)d\xi. \tag{17}$$

Furthermore, the shear-force $Q_2(x)$ and bending moment $M_2(x)$ of the substrate layer can be determined accordingly by integrating (5) and (6) with respect to x from $x = 0$, respectively:

$$Q_2(x) = b\int_0^x g(\xi)d\xi, \tag{18}$$

$$M_2(x) = b\int_0^x \int_0^\xi g(\varsigma)d\varsigma\, d\xi - \frac{bh_2}{2}\int_0^x f(\xi)d\xi. \tag{19}$$

In the above, two BCs of free shear-force and bending moment at $x = 0$ as given in (9i) and (9k) have been implied in the derivations.

2.3. Planar stresses in adherends

2.3.1. Planar stresses in the cover layer

For slender adherends of the single-sided strap joint under consideration, as an approach, the axial normal stress in each adherend can be assumed to be varying linearly. Such axial stress can be specified through the flexural stress formula of classic *Euler–Bernoulli* beams. As a result, the axial stress of the cover layer can be expressed as

$$\sigma_{xx}^{(1)} = \frac{S_1}{bh_1} - \frac{M_1 y_1}{I_1} = p_1 - \frac{1}{h_1}\int_0^x f(\xi)d\xi - \frac{12y_1}{h_1^3}\left[M_0 - \int_0^x \int_0^\xi g(\varsigma)d\varsigma\, d\xi - \frac{h_1}{2}\int_0^x f(\xi)d\xi\right]. \tag{20}$$

Shear stress $\tau_{y_1x}^{(1)}$ of the cover layer can be determined by integrating the 2D equilibrium equation of a representative element:

$$\frac{\partial\sigma_{xx}^{(1)}}{\partial x} + \frac{\partial\tau_{y_1x}^{(1)}}{\partial y_1} = 0, \tag{21}$$

with respect to y_1 from an arbitrary location y to the top surface at $y_1 = h_1/2$:

$$\int_{y_1}^{h_1/2} \frac{\partial \sigma_{xx}^{(1)}}{\partial x} dy_1 + \int_{y_1}^{h_1/2} \frac{\partial \tau_{y_1 x}^{(1)}}{\partial y_1} dy_1 = 0, \tag{22}$$

which leads to

$$\tau_{y_1 x}^{(1)} = -\frac{1}{h_1}\left[\left(\frac{h_1}{2} - y_1\right) - \frac{3}{h_1}\left(\frac{h_1^2}{4} - y_1^2\right)\right] f(x) + \frac{6}{h_1^3}\left(\frac{h_1^2}{4} - y_1^2\right)\int_0^x g(\xi) d\xi. \tag{23}$$

In the above, the traction-free BC: $\tau_{y_1 x}^{(1)}(h_1/2) = 0$ has been carried out. Furthermore, transverse normal stress $\sigma_{y_1 y_1}^{(1)}$ in the cover layer can be calculated by integrating the 2D equilibrium equation:

$$\frac{\partial \sigma_{y_1 y_1}^{(1)}}{\partial y_1} + \frac{\partial \tau_{x y_1}^{(1)}}{\partial x} = 0, \tag{24}$$

with respect to y_1 from an arbitrary location y to the top surface at $y_1 = h_1/2$ as

$$\int_{y_1}^{h_1/2} \frac{\partial \sigma_{y_1 y_1}^{(1)}}{\partial y_1} dy_1 + \int_{y_1}^{h_1/2} \frac{\partial \tau_{x y_1}^{(1)}}{\partial x} dy_1 = 0, \tag{25}$$

which yields

$$\begin{aligned}\sigma_{y_1 y_1}^{(1)} = &-\frac{1}{h_1}\left\{\frac{h_1}{2}\left(\frac{h_1}{2} - y_1\right) - \frac{1}{2}\left(\frac{h_1^2}{4} - y_1^2\right) - \frac{3}{h_1}\left[\frac{h_1^2}{4}\left(\frac{h_1}{2} - y_1\right) - \frac{1}{3}\left(\frac{h_1^3}{8} - y_1^3\right)\right]\right\} f'(x) \\ &+ \frac{6}{h_1^3}\left[\frac{h_1^2}{4}\left(\frac{h_1}{2} - y_1\right) - \frac{1}{3}\left(\frac{h_1^3}{8} - y_1^3\right)\right] g(x).\end{aligned} \tag{26}$$

2.3.2. Planar stresses in the substrate layers

The stress components in the slender substrate layers can be obtained using the same approach. The axial normal stress can be approximated to follow the flexural stress formula of classic *Euler–Bernoulli* beams:

$$\sigma_{xx}^{(2)} = \frac{S_2}{b h_2} - \frac{M_2 y_2}{I_2} = \frac{1}{h_2}\int_0^x f(\xi) d\xi - \frac{12 y_2}{h_2^3}\left[\int_0^x \int_0^\xi g(\varsigma) d\varsigma \, d\xi - \frac{h_2}{2}\int_0^x f(\xi) d\xi\right]. \tag{27}$$

Shear stress $\tau_{y_2 x}^{(2)}$ can be determined through integration of the 2D static equilibrium equation:

$$\frac{\partial \sigma_{xx}^{(2)}}{\partial x} + \frac{\partial \tau_{y_2 x}^{(2)}}{\partial y_2} = 0, \tag{28}$$

with respect to y_2 from the bottom surface $y_2 = -h_2/2$ to an arbitrary location y_2 of the substrate layer such that

$$\int_{-h_2/2}^{y_2} \frac{\partial \sigma_{xx}^{(2)}}{\partial x} dy_2 + \int_{-h_2/2}^{y_2} \frac{\partial \tau_{y_2 x}^{(2)}}{\partial y_2} dy_2 = 0, \tag{29}$$

which leads to

$$\tau_{y_2 x}^{(2)} = -\frac{1}{h_2}\left[\left(y_2 + \frac{h_2}{2}\right) + \frac{3}{h_2}\left(y_2^2 - \frac{h_2^2}{4}\right)\right] f(x) + \frac{6}{h_2^3}\left(y_2^2 - \frac{h_2^2}{4}\right)\int_0^x g(\xi) d\xi. \tag{30}$$

In the above, the stress-free BC: $\tau_{y_2 x}^{(2)}(-h_2/2) = 0$ has been used. Furthermore, normal stress $\sigma_{y_2 y_2}^{(2)}$ in the substrate layer can be determined by integrating the 2D equilibrium equation:

$$\frac{\partial \sigma_{y_2 y_2}^{(2)}}{\partial y_2} + \frac{\partial \tau_{x y_2}^{(2)}}{\partial x} = 0, \tag{31}$$

with respect to y_2 from the bottom surface at $y_2 = -h_2/2$ to an arbitrary location y_2 such that

$$\int_{-h_2/2}^{y_2} \frac{\partial \sigma_{y_2 y_2}^{(2)}}{\partial y_2} dy_2 + \int_{-h_2/2}^{y_2} \frac{\partial \tau_{x y_2}^{(2)}}{\partial x} dy_2 = 0, \tag{32}$$

which further reduces to

$$\sigma^{(2)}_{y_2y_2} = \left\{\frac{1}{h_2}\left[\frac{1}{2}\left(y_2^2 - \frac{h_2^2}{4}\right) + \frac{h_2}{2}\left(y_2 + \frac{h_2}{2}\right)\right] + \frac{3}{h_2^2}\left[\frac{1}{3}\left(y_2^3 + \frac{h_2^3}{8}\right) - \frac{h_2^2}{4}\left(y_2 + \frac{h_2}{2}\right)\right]\right\} f'(x) - \frac{6}{h_2^3}\left[\frac{1}{3}\left(y_2^3 + \frac{h_2^3}{8}\right) - \frac{h_2^2}{4}\left(y_2 + \frac{h_2}{2}\right)\right] g(x). \tag{33}$$

In the above, traction-free BC: $\sigma^{(2)}_{y_2y_2}(-h_2/2) = 0$ has been adopted.

From the above derivation, it can be concluded that with the approximation of axial normal stress varying linearly across the cover and substrate layers, the corresponding statically compatible shear and transverse normal stresses vary parabolically and cubically across the layers, respectively.

2.4. Governing equations of interfacial stress functions and solution

With the above stress components in the cover and substrate layers, strain energy of the right half-joint ($0 \leqslant x \leqslant L$) can be expressed as (Beer et al., 2009; Chen & Cheng, 1983; Wu, Dzenis, & Strabala, 2008)

$$U = b\int_0^L \int_{-h_1/2}^{h_1/2} \left\{\frac{1}{2}\left[\sigma^{(1)}_{xx}\varepsilon^{(1)}_{xx} + \sigma^{(1)}_{yy}\varepsilon^{(1)}_{yy}\right] + \frac{1+\upsilon_1}{E_1}\left(\tau^{(1)}_{xy_1}\right)^2\right\} dx\, dy_1 + b\int_0^L \int_{-h_2/2}^{h_2/2} \left\{\frac{1}{2}\left[\sigma^{(2)}_{xx}\varepsilon^{(2)}_{xx} + \sigma^{(2)}_{yy}\varepsilon^{(2)}_{yy}\right] + \frac{1+\upsilon_1}{E_1}\left(\tau^{(2)}_{xy_2}\right)^2\right\} dx\, dy_2. \tag{34}$$

In the above, $\varepsilon^{(i)}_{xx}$ and $\varepsilon^{(i)}_{yy}(i = 1,2)$ are respectively the axial and transverse normal strains of the adherends defined by generalized Hooke's law of isotropic, linearly thermoelastic solids (in the *plane-stress* state):

$$\varepsilon^{(i)}_{xx} = \frac{1}{E_i}\sigma^{(i)}_{xx} - \frac{\upsilon_i}{E_i}\sigma^{(i)}_{yy} + \alpha_i\Delta T, \tag{35}$$

$$\varepsilon^{(i)}_{yy} = \frac{1}{E_i}\sigma^{(i)}_{yy} - \frac{\upsilon_i}{E_i}\sigma^{(i)}_{xx} + \alpha_i\Delta T, \tag{36}$$

where $\alpha_i(i = 1,2)$ are coefficients of thermal expansion of the upper and lower adherends, respectively, and ΔT is the uniform temperature change of the joint from a reference temperature of thermomechanical-stress free state. Mathematically, strain energy (34) is a functional with respect to the two unknown interfacial stress-functions f and g introduced above. Based on the theorem of minimum complementary strain energy of elastic bodies, the strain energy of the joint reaches a stationary point in the state of static equilibrium, which corresponds to the necessary condition in terms of variation of the strain energy (34) such that (Chen & Cheng, 1983; Timoshenko & Goodier, 1951; Wu et al., 2008)

$$\delta U = 0, \tag{37}$$

i.e.,

$$\delta U = b\int_0^L \int_{-h_1/2}^{h_1/2} \left\{\frac{1}{2}\left[\sigma^{(1)}_{xx}\delta\varepsilon^{(1)}_{xx} + \delta\sigma^{(1)}_{xx}\varepsilon^{(1)}_{xx} + \sigma^{(1)}_{yy}\delta\varepsilon^{(1)}_{yy} + \delta\sigma^{(1)}_{yy}\varepsilon^{(1)}_{yy}\right] + \frac{2(1+\upsilon_1)}{E_1}\tau^{(1)}_{xy_1}\delta\tau^{(1)}_{xy_1}\right\} dx\, dy_1 + b\int_0^L \int_{-h_2/2}^{h_2/2} \left\{\frac{1}{2}\left[\sigma^{(2)}_{xx}\delta\varepsilon^{(2)}_{xx} + \delta\sigma^{(2)}_{xx}\varepsilon^{(2)}_{xx} + \sigma^{(2)}_{yy}\delta\varepsilon^{(2)}_{yy} + \delta\sigma^{(2)}_{yy}\varepsilon^{(2)}_{yy}\right] + \frac{2(1+\upsilon_2)}{E_2}\tau^{(2)}_{xy_2}\delta\tau^{(2)}_{xy_2}\right\} dx\, dy_2. \tag{38}$$

where δ is the mathematical varational operator with respect to either f or g.

By substituting the stress expressions (20), (23), (26), (27), (30) and (33) and normal strains (35) as well as (36) into (38) and performing several variational operations and mathematical simplifications, it turns out that stress-functions f and g satisfy a system of two coupled 4th-order ODEs of constant coefficients:

$$A_{11}F^{(IV)}(\xi) + A_{12}G^{(IV)}(\xi) + B_{11}F''(\xi) + B_{12}G''(\xi) + C_{11}F(\xi) + C_{12}G(\xi) + D_1 = 0, \tag{39a}$$

$$A_{12}F^{(IV)}(\xi) + A_{22}G^{(IV)}(\xi) + B_{12}F''(\xi) + B_{22}G''(\xi) + C_{12}F(\xi) + C_{22}G(\xi) + D_2 = 0, \tag{39b}$$

where

$$F(\xi) = F(x/h_2) = -\frac{1}{p_0h_2}\int_0^x f(\zeta)d\zeta, \tag{40a}$$

$$G(\xi) = G(x/h_2) = \frac{1}{p_0h_2^2}\int_0^x \int_0^\zeta g(\eta)d\eta\, d\zeta, \tag{40b}$$

$$A_{11} = \frac{1}{105}\left(h_{12}^3 + e_{12}\right), \tag{41a}$$

$$A_{12} = \frac{11}{210}\left(-h_{12}^2 + e_{12}\right), \tag{41b}$$

$$A_{22} = \frac{13}{35}(h_{12} + e_{12}), \tag{41c}$$

$$B_{11} = -\frac{4}{15}(h_{12} + e_{12}), \tag{41d}$$

$$B_{12} = \frac{1}{5}[(1 - 5\mu_1) - (1 - 5\mu_2)e_{12}], \tag{41e}$$

$$B_{22} = -\frac{12}{5}\left(h_{12}^{-1} + e_{12}\right), \tag{41f}$$

$$C_{11} = 4\left(h_{12}^{-1} + e_{12}\right), \tag{41g}$$

$$C_{12} = 6\left(-h_{12}^{-2} + e_{12}\right), \tag{41h}$$

$$C_{22} = 12\left(h_{12}^{-3} + e_{12}\right), \tag{41i}$$

$$D_1 = \begin{cases} (3 + 4h_{12})h_{12}^{-2} + \frac{1}{2}(\alpha_1 - \alpha_2)\Delta T E_1/p_0, \\ \quad \text{(for combined mechanical and thermal loads—plane-stress)} \\ (3 + 4h_{12})h_{12}^{-2} + \frac{1}{2}[(1 + \upsilon_1)\alpha_1 - (1 + \upsilon_2)\alpha_2]\Delta T E_1/p_0, \\ \quad \text{(for combined mechanical and thermal loads—plane-strain)} \\ (3 + 4h_{12})h_{12}^{-2}, \quad \text{(for pure mechanical load—either plane-stress or plane-strain)} \\ \frac{1}{2}(\alpha_1 - \alpha_2)\Delta T E_1/p_0, \quad \text{(for pure thermal load—plane-stress)} \\ \frac{1}{2}[(1 + \upsilon_1)\alpha_1 - (1 + \upsilon_2)\alpha_2]\Delta T E_1/p_0, \quad \text{(for pure thermal load—plane-strain)} \end{cases} \tag{41j}$$

$$D_2 = \begin{cases} -6(1 + h_{12})h_{12}^{-3}, & \text{(for pure mechanical or combined mechanical and thermal loads)} \\ 0, & \text{(for pure thermal load)} \end{cases} \tag{41k}$$

$$h_{12} = h_1/h_2, \tag{41l}$$

$$e_{12} = E_1/E_2. \tag{41m}$$

In the above, when the thermomechanical stress of the joint due to pure temperature change is considered, the stress p_0 adopted in the 4th and 5th expressions in (41j) is understood as a stress reference for dimensionless purpose as was initially introduced in (40a) and (40b). In addition, these governing equations can also be applied to the cases of *plane strain* by replacing E_i by $E_i/(1-\upsilon_i^2)$, υ_i by $\upsilon_i/(1-\upsilon_i)$, and α_i by $(1+\upsilon_i)\alpha_i$, where $i = 1, 2$.

Furthermore, the system of dimensionless ODEs (39a) and (39b) can be recast in matrix format:

$$\begin{bmatrix} A_{11} & A_{12} \\ A_{12} & A_{22} \end{bmatrix} \begin{Bmatrix} F^{(IV)}(\xi) \\ G^{(IV)}(\xi) \end{Bmatrix} + \begin{bmatrix} B_{11} & B_{12} \\ B_{12} & B_{22} \end{bmatrix} \begin{Bmatrix} F''(\xi) \\ G''(\xi) \end{Bmatrix} + \begin{bmatrix} C_{11} & C_{12} \\ C_{12} & C_{22} \end{bmatrix} \begin{Bmatrix} F(\xi) \\ G(\xi) \end{Bmatrix} + \begin{Bmatrix} D_1 \\ D_2 \end{Bmatrix} = \begin{Bmatrix} 0 \\ 0 \end{Bmatrix}. \tag{42}$$

The above ODEs can be further expressed in a concise format:

$$[A]\{\Phi^{(IV)}\} + [B]\{\Phi''\} + [C]\{\Phi\} + \{D\} = \{0\}, \tag{43}$$

where [A], [B] and [C] are three 2×2 symmetric real matrices:

$$[A] = [A]^T = \begin{bmatrix} A_{11} & A_{12} \\ A_{12} & A_{22} \end{bmatrix}, \tag{44a}$$

$$[B] = [B]^T = \begin{bmatrix} B_{11} & B_{12} \\ B_{12} & B_{22} \end{bmatrix}, \tag{44b}$$

$$[C] = [C]^T = \begin{bmatrix} C_{11} & C_{12} \\ C_{12} & C_{22} \end{bmatrix}, \tag{44c}$$

and $\{\Phi\}$, {D}, and {0} are three vectors defined as

$$\{\Phi\} = \{F(\xi), G(\xi)\}^T, \tag{45a}$$

$$\{D\} = \{D_1, D_2\}^T, \tag{45b}$$

$$\{0\} = \{0, 0\}^T. \tag{45c}$$

The solution to (43) can be obtained by superimposing the general solution $\{\Psi\}$ of the corresponding set of homogeneous ODEs to a particular solution $\{\Phi_0\}$:

$$\{\Phi\} = \{\Psi\} + \{\Phi_0\}, \tag{46}$$

$$[A]\{\Psi^{(IV)}\} + [B]\{\Psi''\} + [C]\{\Psi\} = \{0\}, \tag{47}$$

$$\{\Phi_0\} = -[C]^{-1}\{D\}. \tag{48}$$

To solve the system of homogeneous ODEs (47), assume the general solution $\{\Psi\}$ to carry the form:

$$\{\Psi\} = \{\Psi_0\}\exp(\lambda\xi), \tag{49}$$

where λ and $\{\Psi_0\}$ are respectively the eigenvalue and eigenvector of the characteristic equation corresponding to (47):

$$\lambda^4[A]\{\Psi_0\} + \lambda^2[B]\{\Psi_0\} + [C]\{\Psi_0\} = \{0\}. \tag{50}$$

In addition, by introducing

$$\{\Psi_1\} = \lambda^2\{\Psi_0\}, \tag{51}$$

the eigenvalue problem (50) can be converted to a generalized eigenvalue problem:

$$\begin{bmatrix} I & 0 \\ 0 & A \end{bmatrix}\begin{Bmatrix} \Psi_0 \\ \Psi_1 \end{Bmatrix} = -\lambda^{-2}\begin{bmatrix} 0 & -I \\ C & B \end{bmatrix}\begin{Bmatrix} \Psi_0 \\ \Psi_1 \end{Bmatrix}, \tag{52}$$

which can be solved efficiently by using robust numerical algorithms available in the literature [e.g. the eig () function provided by Matlab™]. Thus, the final expression of the general solution (46) is

$$\{\Phi\} = \sum_{k=1}^{4}\left[c_k\left\{\Psi_0^k\right\}\exp(\lambda_k\xi) + d_k\left\{\Psi_0^k\right\}\exp(-\lambda_k\xi)\right] + \{\Phi_0\}, \tag{53}$$

where $\left\{\Psi_0^k\right\}(k = 1,2,3,4)$ are eigenvectors attached to eigenvalues $\lambda_k(k = 1,2,3,4)$, respectively, and c_k and $d_k(k = 1,2,3,4)$ are the real or complex constants to be determined in satisfying the traction BCs (8)–(9I). Only eight BCs are linearly independent and can be extracted from (8)–(9I) to determine c_k and $d_k(k = 1,2,3,4)$ such that

$$F(0) = 0, \tag{54a}$$

$$F(L/h_2) = -1, \tag{54b}$$

$$F'(0) = 0, \tag{54c}$$

$$F'(L/h_2) = 0, \tag{54d}$$

$$G(0) = 0, \tag{54e}$$

$$G(L/h_2) = 1/2, \tag{54f}$$

$$G'(0) = 0, \tag{54g}$$

$$G'(L/h_2) = 0. \tag{54h}$$

Consequently, substitution of (53) into (54a)–(54h) leads to a set of eight linear algebraic equations:

$$\sum_{k=1}^{4} c_k\Psi_0^{k,1} + \sum_{k=1}^{4} d_k\Psi_0^{k,1} = -\Phi_0^{(1)}, \tag{55a}$$

$$\sum_{k=1}^{4} c_k\Psi_0^{k,1}\exp(\lambda_k L/h_2) + \sum_{k=1}^{4} d_k\Psi_0^{k,1}\exp(-\lambda_k L/h_2) = -\left[1 + \Phi_0^{(1)}\right], \tag{55b}$$

$$\sum_{k=1}^{4} c_k\lambda_k\Psi_0^{k,1} - \sum_{k=1}^{4} d_k\lambda_k\Psi_0^{k,1} = 0, \tag{55c}$$

$$\sum_{k=1}^{4} c_k\lambda_k\Psi_0^{k,1}\exp(\lambda_k L/h_2) - \sum_{k=1}^{4} d_k\lambda_k\Psi_0^{k,1}\exp(-\lambda_k L/h_2) = 0, \tag{55d}$$

$$\sum_{k=1}^{4} c_k\Psi_0^{k,2} + \sum_{k=1}^{4} d_k\Psi_0^{k,2} = -\Phi_0^{(2)}, \tag{55e}$$

$$\sum_{k=1}^{4} c_k\Psi_0^{k,2}\exp(\lambda_k L/h_2) + \sum_{k=1}^{4} d_k\Psi_0^{k,2}\exp(-\lambda_k L/h_2) = 1/2 - \Phi_0^{(2)}, \tag{55f}$$

$$\sum_{k=1}^{4} c_k \lambda_k \Psi_0^{k,2} - \sum_{k=1}^{4} d_k \lambda_k \Psi_0^{k,2} = 0, \tag{55g}$$

$$\sum_{k=1}^{4} c_k \lambda_k \Psi_0^{k,2} \exp(\lambda_k L/h_2) - \sum_{k=1}^{4} d_k \lambda_k \Psi_0^{k,2} \exp(-\lambda_k L/h_2) = 0. \tag{55h}$$

In the above, $\Psi_0^{k,1}$ and $\Psi_0^{k,2}(k = 1,2,3,4)$ are respectively the first and second elements of the kth eigenvector, and $\Phi_0^{(1)}$ and $\Phi_0^{(2)}$ are the 1st and 2nd elements of the particular solution vector $\{\Phi_0\}$. Moreover, for thermomechanical stress analysis of the joint due to pure temperature change, the right terms of (54b) and (54f) should be zeros, which further influence the right terms of (55b) and (55f) accordingly. Therefore, once $c_k(k = 1,2,3,4)$ and $d_k(k = 1,2,3,4)$ are determined by solving the above system of linear algebraic Eqs. (55a)–(55h) numerically, relations (40a), (40b) and (53) finalize the stress functions f and g as

$$f(x)/p_0 = \sum_{k=1}^{4} c_k \Psi_0^{k,1} \lambda_k \exp(\lambda_k x/h_2) - \sum_{k=1}^{4} d_k \Psi_0^{k,1} \lambda_k \exp(-\lambda_k x/h_2), \tag{56a}$$

$$g(x)/p_0 = \sum_{k=1}^{4} c_k \Psi_0^{k,2} \lambda_k^2 \exp(\lambda_k x/h_2) + \sum_{k=1}^{4} d_k \Psi_0^{k,2} \lambda_k^2 \exp(-\lambda_k x/h_2). \tag{56b}$$

Consequently, with the stress functions f and g given in (56a) and (56b), all planar stresses in the adherends can be determined using the expressions formulated in Section 2.3. It needs to be mentioned that except for the BCs of the single-sided strap joint, all the derivations above are actually independent of the specific configuration of the joint. Thus, the governing Eqs. (39a) and (39b) can be applicable to other statically equivalent bonded joints such as single-lap joint, symmetric bonded joints, etc.

3. Examples and discussions

3.1. Interfacial stresses in a single-strap joint due to mechanical loads

To validate the analytic model formulated in this work, we consider the interfacial shear and normal stresses of a single-sided strap joint subjected to uniform axial tension (in plane-stress state) by using the present method and FEM (ANSYS™), respectively. The single-sided strap joint is assumed to be made of two identical aluminum substrate layers (E_2 = 70 GPa, υ_2 = 0.34) reinforced with a steel cover layer (E_1 = 200 GPa, υ_1 = 0.29). The adherends have the same width; other geometries of the joint are: h_1 = 2 mm (steel), h_2 = 4 mm (aluminum), and L = 20 mm (See Fig. 1). The uniform tensile stress of the substrate layers is assumed to be p_0 = 1 MPa. In the linear FEM stress analysis of the joint using ANSYS™, four-node elements (PLANE182) and mapped uniform quadrilateral meshes are utilized. Also, it needs to be mentioned that near the free-edge of two bonded dissimilar adherends, a stress singularity exists. To track the potential singular stresses near the free edges, FEM simulations based on four mesh sizes (i.e., 0.4 × 0.4 mm, 0.2 × 0.2 mm, 0.1 × 0.1 mm, and 0.05 × 0.05 mm) are considered sequentially. Variations of the interfacial shear and normal stresses with the distance from the left edge are plotted in Fig. 3(a) and (b). It can be observed that due to the bending moment near the mid-span of the joint (See Fig. 1), very high interfacial stresses exist near the free edge. Furthermore, the stress comparison shown in Fig. 3(a) and (b) indicates that the present model is capable of predicting very good stress variations along the interface, especially for the interfacial normal stress.

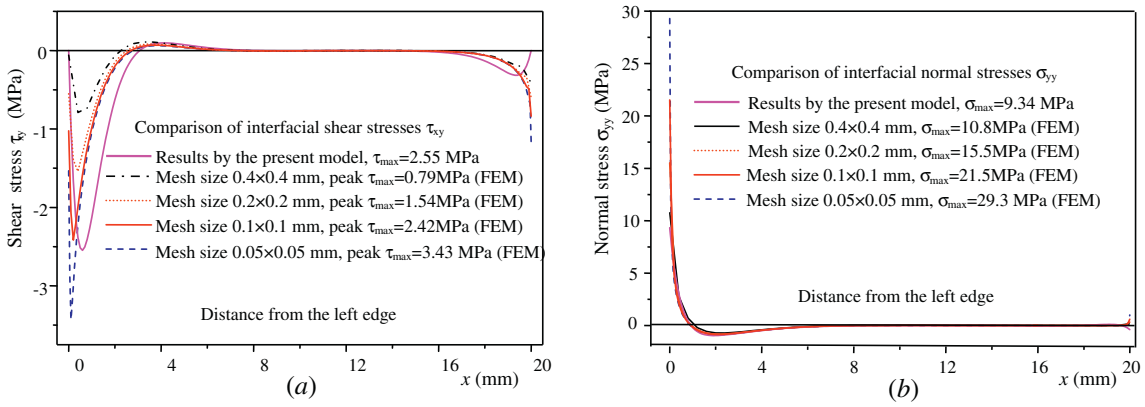

Fig. 3. Comparison of interfacial shear and normal stresses predicted by the present stress-function variational method with those by FEM (ANSYS™): (a) interfacial shear stress τ and (b) interfacial normal stress σ (axial tensile stress of the substrate layers: p_0 = 1 MPa).

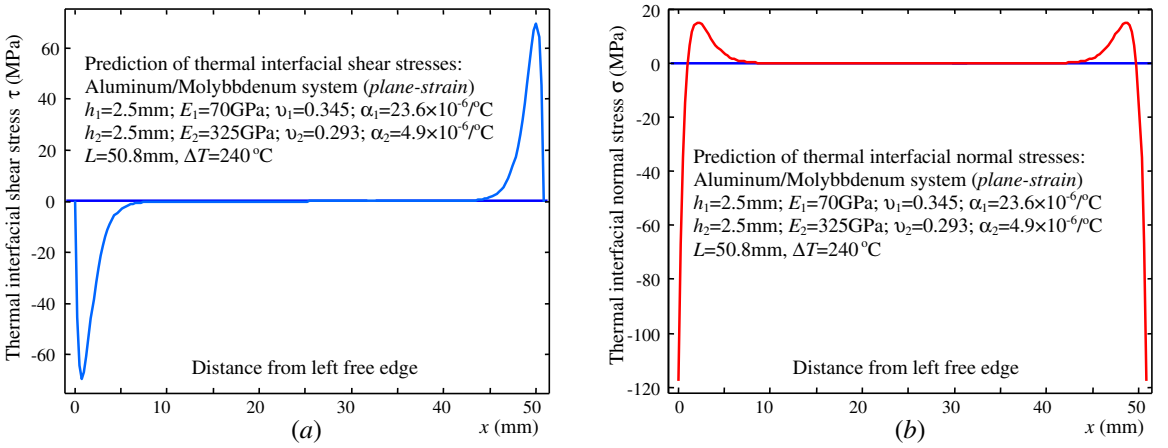

Fig. 4. Variations of the thermomechanical interfacial shear and normal stresses in a bimaterial thermostat subjected to uniform temperature change (ΔT = 240 °C): (a) interfacial shear stress τ and (b) interfacial normal stress σ.

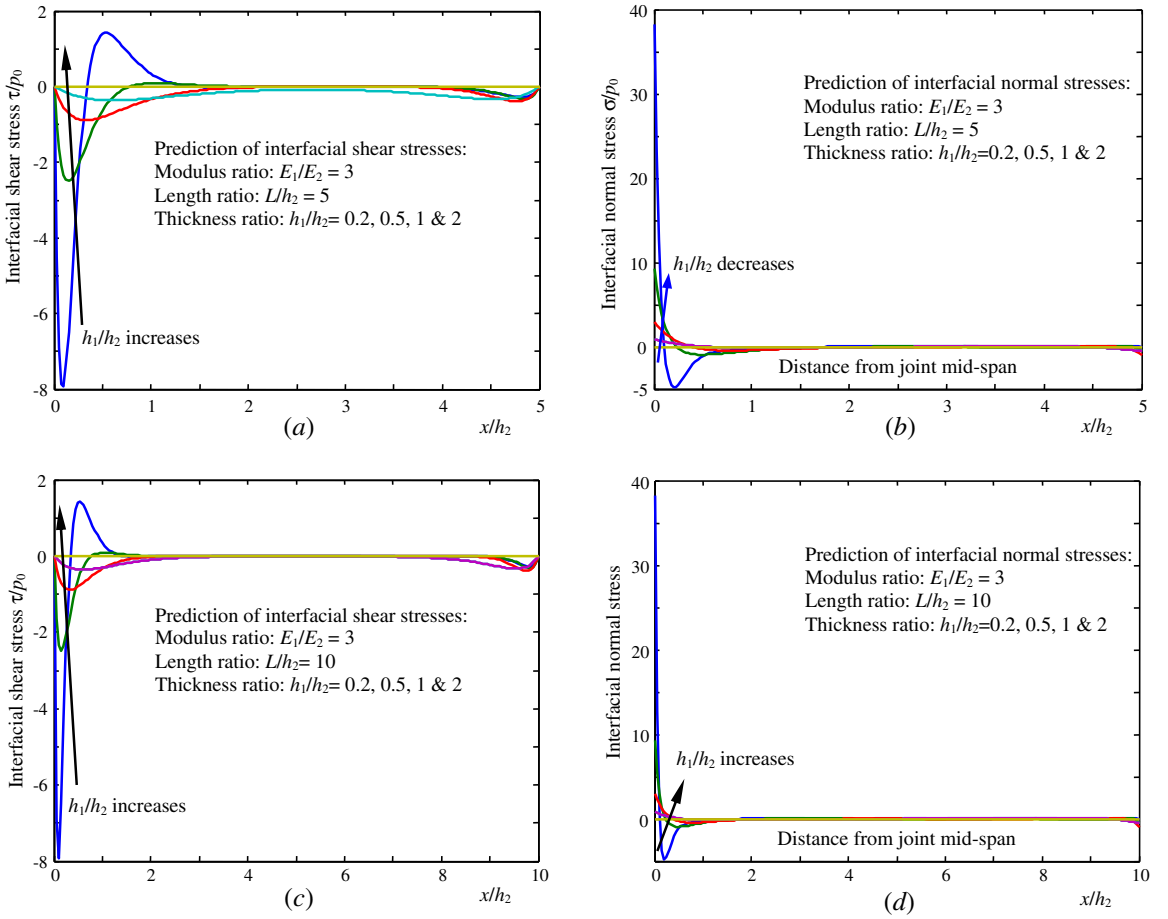

Fig. 5. Variations of the dimensionless interfacial shear and normal stresses in single-sided strap joints with the dimensionless distance from the joint mid-span at varying thickness and length ratios (E_1/E_2 = 3).

In addition, due to the existence of stress singularity near the free-edge, the interfacial stresses predicted by FEM increase rapidly with decreasing mesh size. Like most analytic models available in the literature, the present model is unable to predict such singularity. However, the very good fitting to the interfacial stress variations predicted by FEM confirms the validity of the present model that can be utilized for scaling analysis, design and optimization of joint structures, among others.

3.2. Thermal interfacial stresses in a bimaterial thermostat

It has been mentioned that thermomechanical stress analysis of a single-sided strap joint (see Fig. 1) due to a pure temperature change is equivalent to that of a bimaterial thermostat. To validate the present model, herein we consider the thermomechanical stress analysis of an aluminum/molybdenum thermostat subjected to a uniform temperature change as studied by Suhir (1989a, 1989b), Ru (2002), Eischen, Chung, and Kim (1990). In terms of the symbol system utilized in this work, the system parameters are: $h_1 = 2.5$ mm, $E_1 = 70$ GPa, $\upsilon_1 = 0.345$, $\alpha_1 = 23.6 \times 10^{-6}/^{\circ}$C, $h_2 = 2.5$ mm, $E_2 = 325$ GPa, $\upsilon_2 = 0.293$, $\alpha_2 = 4.9 \times 10^{-6}/^{\circ}$C, $L = 50.8$ mm and $\Delta T = 240\ ^{\circ}$C (Eischen et al., 1990; Ru, 2002; Suhir, 1989a, 1989b). A *plane-strain* state is assumed in the simulation based on the present model. Fig. 4(a) and (b) show the distribution of thermomechanical interfacial shear and normal stresses along the interface, respectively. It can be observed that the shear and peeling stresses are highly localized at the free edges. Specifically, the peak value of interfacial shear stress $\tau_{max} = 69.32$ MPa appears at a distance close to $L/20$ from the free edges which is very close to the one by Ru (2002) ($\tau_{max} = 70$ MPa); the peak value of interfacial normal stress $\sigma_{max} = 117.70$ MPa occurs at the free edges which is slightly higher than those predicted by Ru (2002) and Eischen et al. (1990) while lower than that given by Suhir (1989a, 1989b). Stress variations along the interface and locations of the peak stresses match the literature results very well (Eischen et al., 1990; Ru, 2002). Thus, the above comparisons confirm the reliability of the present method.

3.3. Scaling analysis of interfacial stresses

Now let us further examine dependencies of the interfacial mechanical and thermomechanical stresses upon geometries and material properties of the single-sided strap joint including layer thickness ratio h_1/h_2, length ratio L/h_2, modulus ratio E_1/E_2, and coefficients of thermal expansion α_1 and α_2. In the current study of linearly thermoelastic joints, the joint stresses due to mechanical loads and temperature change can be obtained through linear superposition and therefore dealt with separately for convenience of scaling analysis and practical applications.

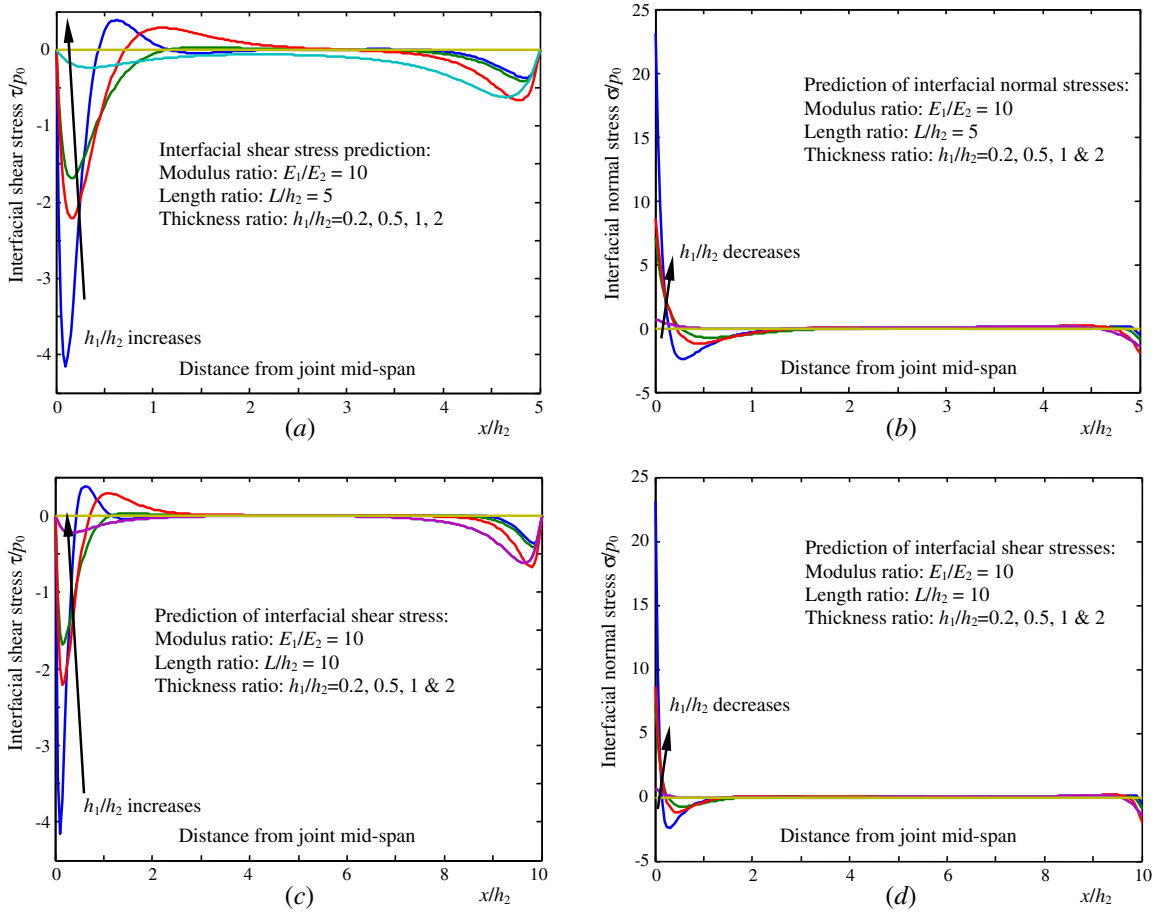

Fig. 6. Variations of the dimensionless interfacial shear and normal stresses in single-sided strap joints with the dimensionless distance from the joint mid-span at varying thickness and length ratios ($E_1/E_2 = 10$).

3.3.1. Scaling analysis of interfacial stresses due to mechanical loads

For the scaling analysis of mechanical stresses in the joint, four thickness ratios ($h_1/h_2 = 0.2, 0.5, 1, 2$), two length ratios ($L/h_2 = 5, 10$), and two modulus ratios ($E_1/E_2 = 3, 10$) are adopted; Poisson's ratios of the adherends are fixed as $\upsilon_1 = 0.345$ and $\upsilon_2 = 0.293$. In this case, the joint is considered in a *plane-stress* state. Figs. 5 and 6 show variations of the dimensionless interfacial shear stress τ/p_0 and normal (peeling) stress σ/p_0 with the dimensionless distance x/h_2 from the joint mid-span at varying length and modulus ratios, respectively. It can be observed that the interfacial shear and normal stresses have high stress concentrations near the interior edges of the adherends and the shear stresses satisfy the shear-free BC at two adherend ends. Due to the existence of a bending moment at the mid-span, as illustrated in Fig. 1, the peak value of interfacial normal stress at the interior edges is much larger than that of the shear stress in all the cases under examination; the stress concentration of both the interfacial shear and normal stresses at the interior edges is much higher than that at the exterior edges. Thus, it can be concluded that for single-sided strap joints, debonding failure at the mid-span due to the high peeling stress is the main failure mode. Such high stress concentration can be mechanically suppressed by using double-sided strap joints to eliminate the potential bending moment and related larger defection at the mid-span.

In addition, Figs. 5 and 6 also show that for fixed modulus and thickness ratios of the single-sided strap joint, the length ratio L/h_2 (i.e., ratio of the cover layer length vs. the thickness of substrate layers) does not appreciably influence the interfacial stress variation; however both the thickness and modulus ratios of the adherends significantly affect the interfacial stress variation. For given length ratio L/h_2, higher flexural rigidity of the cover layer due to either larger modulus ratio (E_1/E_2) or larger thickness ratio h_1/h_2 can lead to a lower stress concentration of both the interfacial shear and normal stresses. The reason is that stiffer cover layer can suppress the larger deflection of the cover layer at the mid-span and therefore decreases the deflection-induced higher shear and peeling stresses near the interior edges. Thus, stiffer and thicker cover layers are favorable to enhance mechanical durability of single-sided strap joints.

3.3.2. Scaling analysis of interfacial stresses due to a pure temperature change

The derivation in Section 2 has indicated that thermomechanical stress analysis of a single-sided strap joint due to a pure temperature change is equivalent to that of a bimaterial thermostat. For the scaling analysis of thermomechanical stresses in

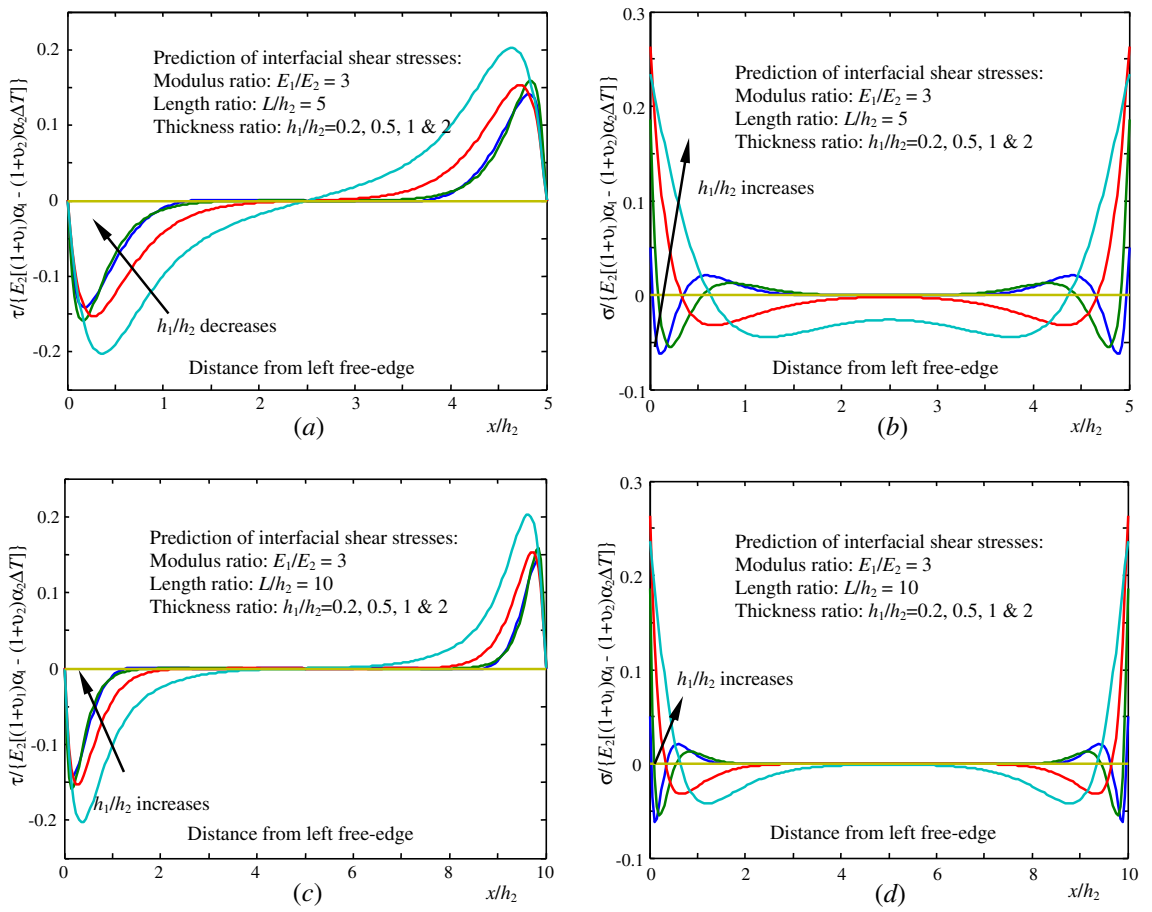

Fig. 7. Variations of the dimensionless thermomechanical interfacial shear and normal stresses in a bimaterial thermostat with the dimensionless distance from the right free-edge at varying thickness and length ratios ($E_1/E_2 = 3$).

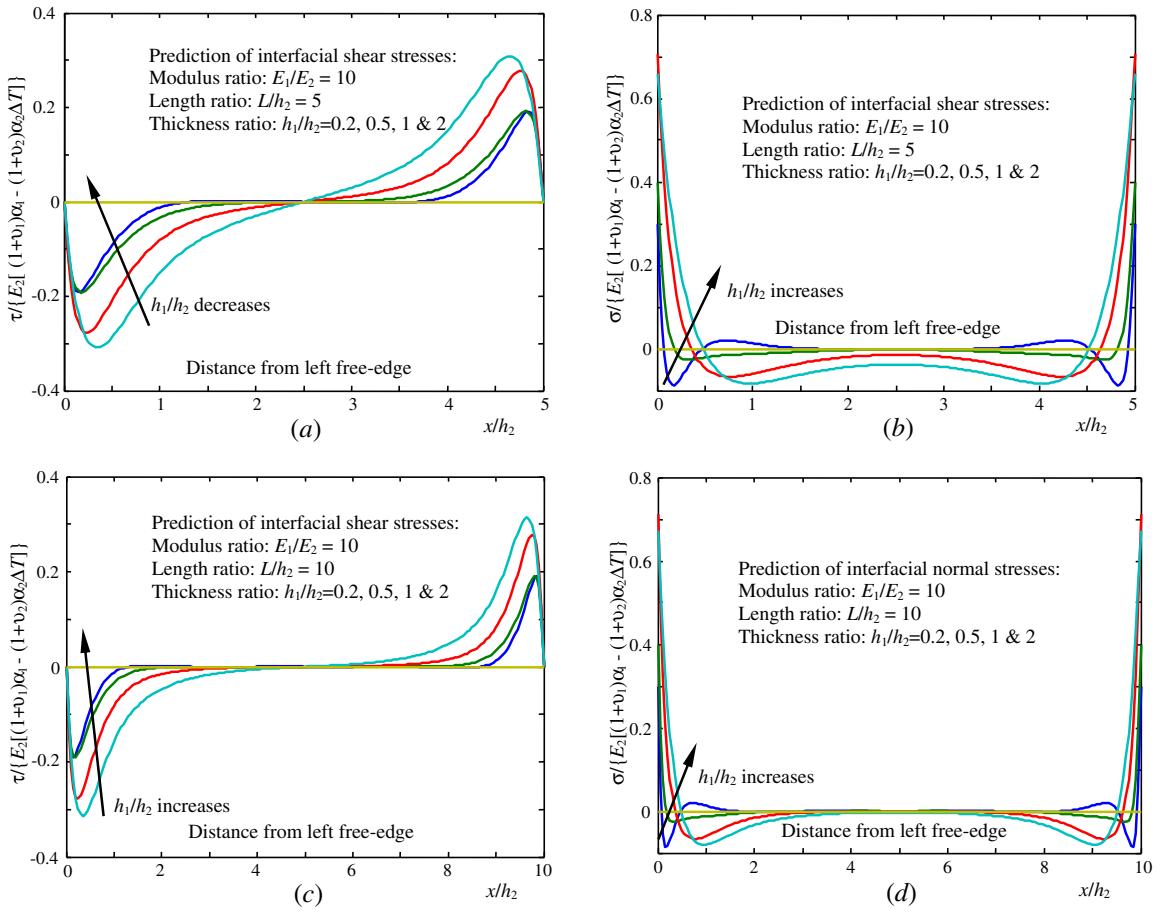

Fig. 8. Variations of the dimensionless thermomechanical interfacial shear and normal stresses in a bimaterial thermostat with the dimensionless distance from the left free-edge at varying thickness and length ratios (E_1/E_2 = 10).

such a bimaterial thermostat, the above parameter ratios are further adopted in the simulations. In this case, the thermostat is considered in a *plane-strain* state for the particular interest of electronic packaging. Figs. 7 and 8 show variations of the dimensionless interfacial shear stress $\tau/\{E_2[(1+\upsilon_1)\alpha_1-(1+\upsilon_2)\alpha_2]\Delta T\}$ and normal (peeling) stress $\sigma/\{E_2[(1+\upsilon_1)\alpha_1-(1+\upsilon_2)\alpha_2]\Delta T\}$ with the dimensionless distance x/h_2 from the joint mid-span at varying length and modulus ratios. It can be observed that the shear stress is antisymmetric while the normal stress is symmetric with respect to the quarter-span of the cover layer (or the mid-span of the equivalent bimaterial thermostat). Similar to the case of pure mechanical stress [see Figs. 5 and 6], the length ratios L/h_2 under investigation do not clearly affect the thermal interfacial shear and normal stress variation; however the thickness and modulus ratios noticeably influence the thermomechanical interfacial stresses.

It can be detected from Figs. 7 and 8 that for the given modulus ratios (e.g. E_1/E_2 = 3 and 10 such that the cover layer is stiffer than the substrate layer), the peak value of the thermomechanical interfacial shear-stress decreases with decreasing thickness ratio (h_1/h_2); in contrast the peak value of normal stress occurring at adherend ends increases with decreasing thickness ratio (h_1/h_2). In this case, the thicker the cover layer is, the larger the bending stiffness of the thermostat is. The larger stiffness of the cover layer leads to higher bending flexural stress and therefore higher interfacial normal stress and lower sliding (i.e., lower shearing strain near the interface) for a given mismatch of thermal strains. In addition, for a fixed thickness ratio (h_1/h_2), the peak value of either the thermomechanical interfacial shear or normal stress increases remarkably with increasing modulus ratio (E_1/E_2). This can be understood that the mismatch of the coefficients of thermal expansion of the adherends leads to a mismatch of thermal strains when subjected to a temperature change that further induces the bending of the thermostat. As a result, the larger the modulus ratio is, the higher the thermal stress is. Furthermore, the peak value of the thermomechanical interfacial normal stress is larger than that of shear stress. This phenomenon is more pronounced with the increase of modulus ratio (E_1/E_2). The above scaling analysis indicates that interface debonding due to high peeling stress is the dominate failure mode of bimaterial thermostats.

In addition, the solving process for the eigenvalue problem (52) and the set of linear algebraic equations can be performed conveniently by designing a concise computational code such as using Matlab™. Compared to FEM, this method is more efficient for stress analysis of bonded joints since it only requires the input of basic dimensions and material properties. Thus,

the present method is an efficient, reliable method for scaling analysis, sensitivity analysis of design parameters, and optimal design of bonded joints. This method can also be easily extended to stress analysis of other joints.

4. Concluding remarks

A novel stress-function variational method has been successfully formulated to approach the interfacial stresses of bonded joints subjected to mechanical or thermomechanical loads. In the process, the axial normal stresses are approached as linearly varying across the adherend layers based on the flexural stress formula of the elementary beam theory, while the planar shear and transverse normal stresses are determined by exactly satisfying the 2D stress equilibrium equations. The deformation compatibility of the joints is satisfied in the sense of minimization of the complementary strain energy of the joint. A set of governing ODEs has been developed, which can be used for stress analysis of a variety of bonded joints made of two adherends for joint design, structural optimization, and interfacial damage evaluation. Advantages of the current interfacial stress solutions include that all the BCs are satisfied exactly and all the material and geometrical parameters have been incorporated into the model. This offers an improved understanding of the scaling behavior of stress variation in bonded joints. The analytic formalism developed in this work can be conveniently generalized for a variety of bonded structures and layered materials where interfacial stresses dictate their strength and reliability.

Acknowledgments

Partial support of this work by the Centennial Endowment Fund of NDSU Development Foundation and the Faculty Research Initiative Grant is gratefully appreciated.

References

Beer, F., Johnston, E. R., Dewolf, J. T., & Mazurek, D. F. (2009). *Mechanics of materials* (5th ed.). New York, USA: McGraw Hill.
Chen, D., & Cheng, S. (1983). An analysis of adhesive-bonded single-lap joints. *Journal of Applied Mechanics – Transactions of the ASME, 50*, 109–115.
Chen, W. T., & Nelson, C. W. (1979). Thermal stress in bonded joints. *IBM Journal of Research and Development, 23*, 179–188.
da Silva, L. F. M., das Neves, P. J. C., Adams, R. D., & Spelt, J. K. (2009a). Analytical models of adhesively bonded joints – Part I: Literature survey. *International Journal of Adhesion and Adhesives, 29*, 319–330.
da Silva, L. F. M., das Neves, P. J. C., Adams, R. D., Wang, A., & Spelt, J. K. (2009b). Analytical models of adhesively bonded joints – Part II: Comparative study. *International Journal of Adhesion and Adhesives, 29*, 331–341.
Delale, F., Erdogan, F., & Aydinoglu, M. N. (1981). Stresses in adhesively bonded joints: a closed-form solution. *Journal of Composite Materials, 15*, 249–271.
Diaz, A. D., Hadj-Ahmed, R., Foret, G., & Ehrlacher, A. (2009). Stress analysis in a classical double lap, adhesively bonded joint with a layerwise model. *International Journal of Adhesion and Adhesives, 29*, 67–76.
Eischen, J. W., Chung, C., & Kim, J. H. (1990). Realistic modeling of edge effect stresses in bimaterial elements. *Journal of Electronic Packaging – Transactions of the ASME, 112*, 16–23.
Goland, M., & Reissner, E. (1944). The stresses in cemented joints. *Journal of Applied Mechanics – Transactions of the ASME, 11*, 17–27.
Hart-Smith, L. J. (1973a). *Adhesive-bonded single-lap joints*. NASA CR-112236.
Hart-Smith, L. J. (1973b). *Adhesive-bonded double-lap joints*. NASA CR-112235.
Her, S. C. (1999). Stress analysis of adhesively-bonded lap joints. *Composites Structure, 47*, 673–678.
Hutchinson, J. W., & Suo, Z. (1992). Mixed mode cracking in layered materials. *Advanced Applied Mechanics, 29*, 63–191.
Jiang, H. Q., Khang, D. Y., Fei, H. Y., Kim, H., Huang, Y. G., Xiao, J. L., & Rogers, J. A. (2008). Finite width effect of thin-films buckling on compliant substrate: experimental and theoretical studies. *Journal of Mechanics and Physics of Solids, 56*, 2585–2598.
Jiang, H. Q., Khang, D. Y., Song, J. Z., Sun, Y. G., Huang, Y. G., & Rogers, J. A. (2007). Finite deformation mechanics in buckled thin films on compliant supports. *Proceedings of the National Academy of Sciences, 104*, 15607–15612.
Khang, D. Y., Jiang, H. Q., Huang, Y., & Rogers, J. A. (2006). A stretchable form of single-crystal silicon for high-performance electronics on rubber substrates. *Science, 311*, 208–212.
Khang, D. Y., Rogers, J. A., & Lee, H. H. (2009). Mechanical buckling: mechanics, metrology, and stretchable electronics. *Advanced Functional Materials, 19*, 1526–1536.
Kim, D. H., & Rogers, J. A. (2008). Stretchable electronics: materials strategies and devices. *Advanced Materials, 20*, 4487–4892.
Lee, J., & Kim, H. (2005). Stress analysis of generally asymmetric single lap adhesively bonded joints. *Journal of Adhesion, 81*, 443–472.
Li, X. F. (2001). Closed-form solution for a mode-III interface crack between two bonded dissimilar elastic layers. *International Journal of Fracture, 109*, L3–L8.
Li, X. F., & Lee, K. Y. (2009). Closed-form solution for an orthotropic elastic strip with a crack perpendicular to the edges under arbitrary anti-plane shear. *Zeitschrift fur Angewandte Mathematik and Mechanik (ZAMM), 89*, 370–382.
Lu, N. S., Yoon, J. I., & Suo, Z. G. (2007). Delamination of stiff islands patterned on stretchable substrates. *International Journal of Materials Research (Z. Metallkd.), 98*, 717–722.
Mortensen, F., & Thomsen, O. T. (2002). Analysis of adhesive bonded joints: a unified approach. *Composite Science and Technology, 62*, 1011–1131.
Ru, C. Q. (2002). Interfacial thermal stresses in bimaterial elastic beams: modified beam models revisited. *Journal of Electronic Packaging – Transactions of the ASME, 124*, 141–146.
Sih, G. C. (1973). *Handbook of Stress Intensity Factors*. Bethlehem, Pennsylvania, USA: Lehigh University.
Song, J., Jiang, H., Liu, Z. J., Khang, D. Y., Huang, Y., Rogers, J. A., Lu, C., & Koh, C. G. (2008). Buckling of a stiff thin film on a compliant substrate in large deformation. *International Journal of Solids and Structures, 45*, 3107–3121.
Suhir, E. (1986). Stresses in bi-material thermostats. *Journal of Applied Mechanics – Transactions of the ASME, 53*, 657–660.
Suhir, E. (1989a). Interfacial stresses in bimaterial thermostats. *Journal of Applied Mechanics – Transactions of the ASME, 56*, 596–600.
Suhir, E. (1989b). Thermally induced interfacial stresses in elongated bimaterial plates. *Applied Mechanics Review, 42*, S253–S262.
Suhir, E. (1991). Approximate evaluation of the elastic interfacial stresses in the thin films with application to High-T_c superconducting ceramics. *International Journal of Solids and Structures, 27*, 1025–1034.
Suhir, E. (2001). Analysis of interfacial thermal stresses in a trimaterial assembly. *Journal of Applied Physics, 89*, 3685–3694.
Suhir, E., & Vujosevic, M. (2010). Bi-material assembly subjected to tensile forces and bending moments applied to the ends of one of its components. *Journal of Solid Mechanics and Material Engineering, 4*, 493–507.
Sun, Y. G., Choi, W. M., Jiang, H. Q., Huang, Y. G. Y., & Rogers, J. A. (2006). Controlled buckling of semiconductor nanoribbons for stretchable electronics. *Natural Nanotechnology, 1*, 201–207.

Suo, Z. G. (2003). Reliability of interconnect structures. In W. Gerberich & W. Yang (Eds.). *Interfacial and nanoscale failure* (Vol. 8, pp. 265–324). Amsterdam, Netherland: Elsevier.
Suo, Z. G., & Hutchinson, J. W. (1990). Interface crack between two elastic layers. *International Journal of Fracture, 43*, 1–18.
Tada, H., Paris, P. C., & Irwin, C. G. (1973). *The stress analysis of cracks*. Hellertown, Pennsylvania, USA: Del Research Corporation.
Timoshenko, S. (1925). Analysis of bi-metal thermostats. *Journal of the Optical Society of America, 11*, 233–255.
Timoshenko, S., & Goodier, J. N. (1951). *Theory of elasticity* (2nd ed.). New York, USA: McGraw-Hill.
Tsai, M. Y., Hsu, C. H., & Han, C. N. (2004). A note on Suhir's solution of thermal stresses for a die-substrate assembly. *Journal of Electronic Packaging – Transactions of the ASME, 126*, 115–119.
Tsai, M. Y., Oplinger, D. W., & Morton, J. (1998). Improved theoretical solutions for adhesive lap joints. *International Journal of Solids and Structures, 35*, 1163–1185.
Volkersen, O. (1938). Die Nietkraftverteilung in zugbeanspruchten Nietverbindungen mit konstanten Laschenquerschnitten. *Luftfahrtforschung, 15*, 41–47.
Wu, X. F., & Dzenis, Y. A. (2002). Closed-form solution for a mode-III interfacial edge crack between two bonded dissimilar elastic strips. *Mechanics Research Communications, 29*, 407–412.
Wu, X. F., Dzenis, Y. A., & Fan, T. Y. (2003). Two semi-infinite interfacial cracks between two bonded dissimilar elastic strips. *International Journal of Engineering Science, 41*, 1699–1710.
Wu, X. F., Dzenis, Y. A., & Gokdag, E. (2004). Edge-cracked orthotropic bimaterial butt joint under anti-plane singularity. *International Journal of Nonlinear Science and Numerical Simulations, 5*, 347–354.
Wu, X. F., Dzenis, Y. A., & Strabala, K. W. (2008). Free-edge stresses and progressive cracking in surface coatings of circular torsion bars. *International Journal of Solids and Structures, 45*, 2251–2264.
Wu, X. F., Dzenis, Y. A., & Zou, W. S. (2003). Interfacial edge crack between two bonded dissimilar orthotropic strips under antiplane point loading. *Zeitschrift fur Angewandte Mathematik and Mechanik (ZAMM), 83*, 419–422.
Wu, X. F., Lilla, E., & Zou, W. S. (2002). A semi-infinite interfacial crack between two bonded dissimilar elastic strips. *Archives of Applied Mechanics, 72*, 630–636.
Yu, H. H., He, M. Y., & Hutchinson, J. W. (2001). Edge effects in thin film delamination. *Acta Materials, 49*, 93–107.
Yu, H. H., & Hutchinson, J. W. (2003). Delamination of thin film strips. *Thin Solid Films, 423*, 54–63.